J Nanostruct 16(4): 4523-4532, Autumn 2026

RESEARCH PAPER

Structural Analysis, Adsorption Behavior, and DFT Study of Alizarin on CuO-αFe$_2$O$_3$ Nanocomposite

Mudeer Mubarak Merza [1], Basma Esam Jasim [2], Rasha M. Dadoosh [1], Nibras Abdul-Ameer Aboud [2], Ali J. Al-Sarray [3]*

[1] *Department of Chemistry, College of Science, Mustansiriyah University, Baghdad, Iraq*

[2] *Department of Chemical and Petroleum Industries Engineering Techniques, Polytechnic College of Engineering Specializations, Middle Technical University, Baghdad, Iraq*

[3] *Polymer Research Unit, College of Science, Mustansiriyah University, Baghdad, Iraq*

ARTICLE INFO

Article History:
Received 05 April 2026
Accepted 10 July 2026
Published 01 October 2026

Keywords:
Adsorption
Alizarin removal
CuO-αFe$_2$O$_3$ nanocomposite
DFT
Structural characterization

ABSTRACT

A novel nanocomposite of the synergetic effect of CuO and αFe$_2$O$_3$ was firstly synthesized and died for alizarin dye (ALZ) removal from aqueous solution as studied in this work. X-ray Diffraction (XRD) and Scanning Electron Microscopy (SEM) analyses revealed distinct structural characteristics of the nanocomposite, with the crystallite size ranged 13.96 nm in average. The results of the adsorption experiments, which produced fits to the Freundlich isotherm model, indicated that this nanocomposite was effective for ALZ removal. Thermodynamic investigations showed that the adsorption is favoured and endothermic, as indicated by enthalpy change ΔH 0 values. Molecular insights into adsorption mechanism were obtained from computational modeling (Density Functional Theory -DFT calculations). The energy gap of CuO-αFe$_2$O$_3$ composite is increased from 1.49 eV to 2.47 eV after the adsorption behaviour of ALZ molecule, suggesting that more stable process occurs during adsorption action. In addition, the energy of chemical adsorption is much more negative than that of physical adsorption, which reveals that hydrogen transfer through chemisorption is more favorable from a thermodynamic perspective. The coalesced experimental-theoretical work reported here will help develop novel environmental adsorbents aimed at practical uses of CuO-αFe$_2$O$_3$ nanocomposites in various fields.

How to cite this article
Merza M., Jasim B., Dadoosh R., Aboud N., Al-Sarray A. Structural Analysis, Adsorption Behavior, and DFT Study of Alizarin on CuO-αFe$_2$O$_3$ Nanocomposite . J Nanostruct, 2026; 16(4):4523-4532. DOI: 10.22052/JNS.2026.04.003

INTRODUCTION

Metal oxide nanostructures are crucial since they have key importance in various sectors. Among these nanostructures, copper(II) oxide, CuO is known to possess lowest energy gap of around 1.20 eV and possesses optimum potential. Due to the strong dependency of material performance on morphology, this highly tunable property has been a boon in various applications such as supercapacitors (SC), batteries, solar cells and catalysts [1-4].

A wide range of CuO nanostructures have been constructed using diverse techniques such as hydrothermal and solvothermal treatments.

* *Corresponding Author Email: basmaisam@mtu.edu.iq*

Furthermore, the interesting features of CuO (cost-effective, abundant materials with non-toxicity in combination with heat tolerance and availability) make it more attractive [5, 6]. Recent advances highlight the effectiveness of the nanocomposite/p-n junction method, providing great potential for photocatalytic and solar-related applications. Enhanced photochemical properties (e.g. light-driven splitting of electrons) is observed for composite metal oxide nanomaterials; thus, in the case of zinc oxide even with subsequent n-suapded hydrothermal growth can show the synergistic CoO effect with CuO [7-11].

Another inorganic compound that has bandgap of 2.10 eV is hematite (Fe2O3), which was used in nano-composites synthesized through several methods where formations at the nanoscale showed distinct properties, adding to its potential as a versatile material. Nanostructures made of different materials have attracted even more attention in the last few years for their possible applications in adsorption processes and have been designed as nanohybrids to treat pollutants Solvent separated multiple atoms (metal, metal oxides) [12-19]. In this study, alizarin dye (ALZ) was chosen as the targeted adsorbate because it is widely used in the textile and dyeing industries and a major source of environmental pollution. Alizarin is a common type of synthetic dye used in textile industries with an anthraquinone framework responsible for significant permanent color properties leading to difficulty in elimination from wastewater using traditional treatment approaches. This property makes them a perfect target for testing new material with high adsorption potential [20-22]. Chemists, chemical engineers, biochemists and physicists use the DFT calculation to predict energies, chemical structures, spectroscopic characteristics of materials, and perform detailed calculations based upon quantum mechanics. DFT calculations are suitable for theoretical studies of various chemical processes on the electron density-dependent parameters with adsorbents and corrosion that includes a large class of materials [23, 24].

This study is designed to synthesize a CuO-αFe_2O_3 nanocomposite with enhanced functionalization and explore its adsorption capacity for alizarin dye (ALZ) in aqueous solutions. The investigation employs a dual approach, utilizing both practical and theoretical methods by leveraging the predictive power of DFT calculations alongside the practical laboratory experiments.

MATERIALS AND METHODS

Chemicals and reagents

All reagents employed throughout this work were of analytical grade and obtained from Sigma-Aldrich. The chemicals were used as received without any additional purification steps.

Synthesis of CuO-αFe_2O_3 Nanocomposite

A 0.05 M aqueous solution of copper(II) acetate monohydrate ($Cu(CH_3COO)_2 \cdot H_2O$) was prepared by dissolving the salt in 100 mL of deionized water· Subsequently, 0·1 g of polyvinylpyrrolidone (PVP, $(C_6H_9NO)_n$) was added to the solution, followed by vigorous stirring for 10 minutes. Afterward, 0.3 mg of iron(III) nitrate nonahydrate ($Fe(NO_3)_3 \cdot 9H_2O$) was introduced into the mixture·

The obtained solution was then mixed with 100 mL of 0.05 M NaOH solution under continuous stirring for 50 minutes. The reaction mixture was maintained at 80 °C for 2 hours. The resulting precipitate was separated by centrifugation and dried at 100 °C for 2 hours. Finally, the dried product was calcined at 450 °C to obtain the CuO–αFe_2O_3 nanocomposite.

Adsorption Experiments

Batch adsorption experiments were conducted using deionized water containing 20 mg/L of alizarin dye (ALZ). The solution was appropriately diluted to achieve the desired concentration. All experiments were carried out in glass tubes with 50 ml of dye solution and 0.01 g of CuO-**αF**e_2O_3. The glass tubes were subjected to 60 minutes of shaking at various temperatures (20, 25, 30, 35, and 40 ℃) using a shaker (HZQ-C). The concentration of the dye in the liquid phase was measured using a UV-visible spectrophotometer. The adsorption capacity (Qe) was determined using Eq. 1 [25, 26].

$$Q_e = \frac{(C_0 - C_e) \times V_{sol}}{M} \quad (1)$$

Here, Qe represents the equilibrium adsorption capacity (mg/g), C_0 and C_e are the initial and equilibrium concentrations of ALZ (mg/L), respectively, V_{sol} is the solution volume (L), and M is the mass of the nanocomposite as the adsorbent (g).

Isotherm of Adsorption

The isotherm of adsorption plays a crucial

role in characterizing the adsorption process of a material. In our study, adsorption isotherms were employed to monitor the release of unwanted chemicals from aqueous media by solid-phase adsorption at a constant temperature. One of the models used in this study is Langmuir isotherm which represented in the Eq. 2 [27,28].

$$\frac{C_e}{Q_e} = \left(\frac{1}{K_L \times Q_m}\right) + \frac{C_e}{Q_m} \quad (2)$$

Where C_e is the adsorbate concentration at equilibrium (mg/L), Q_e is the adsorption capacity at equilibrium (mg/g), Q_{max} is the maximum adsorption capacity (mg/g), and K_L is Langmuir constant (L/mg).

Eq. 3 represents the Freundlich isotherm [29, 30].

$$\log(Q_e) = \log(k_f) + \frac{1}{n}\log(C_e) \quad (3)$$

n and k_f are representing the Freundlich constants as the strength and ability of adsorption, respectively. In addition, Eq. 4 was used to determine the thermodynamic parameters such as entropy changes (ΔS), free energy (ΔG), and enthalpy (ΔH) [31, 32].

$$\log x_m = \frac{-\Delta H}{2.303R} + \frac{\Delta S}{R} \quad (4)$$

Here, T represents the Temperature in (K), R represents the gas constant, and x_m represents the max adsorbed amount in (mg/g).

DFT Calculations

The density functional theory (DFT) calculations were done using B3LYP basis set with a size of 311++G(d, p) to estimate the optimized molecular structures of the studied molecules in a vacuum medium. This basis set was selected due to the accuracy with high computational performance according to similar systems [33, 34]. The frontier molecular orbitals, including the highest unoccupied molecular orbital (HOMO), lowest occupied molecular orbital (LUMO), energy gap, and other energy parameters were obtained based on Koopman's theorem [35]. The calculations were conducted using Gaussian 09 package and visualized through GaussView 5.0 [36, 37]. A monomer of CuO-αFe_2O_3 was selected and optimized in order to simplify the calculations and investigate its interaction with alizarin molecule.

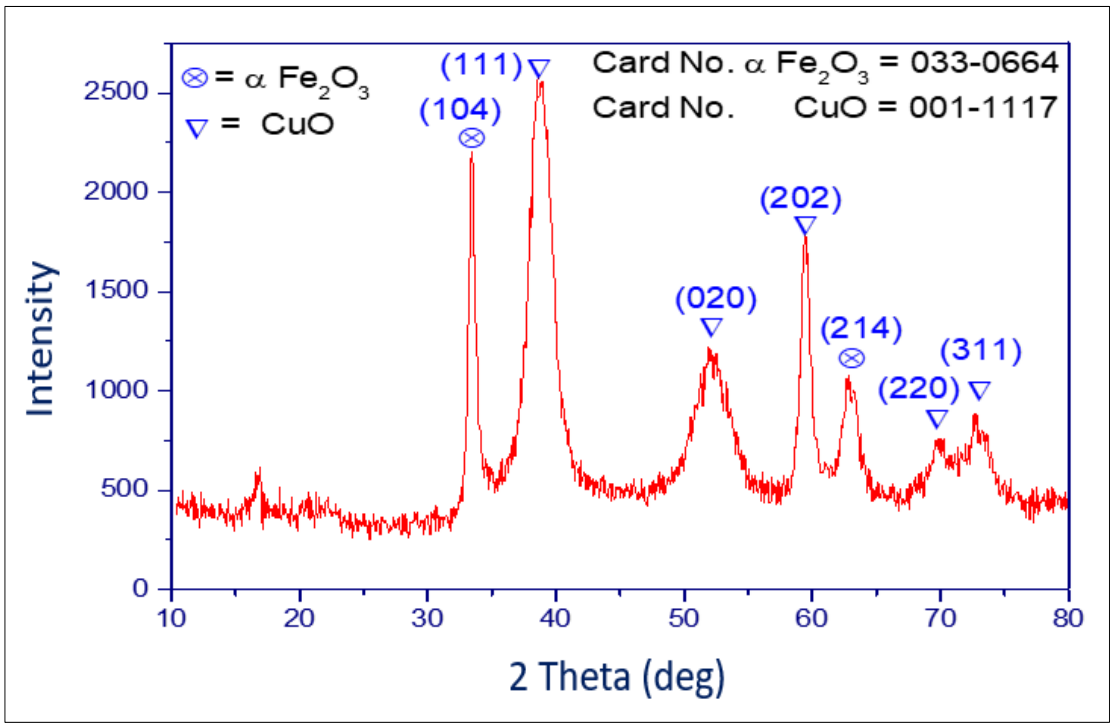

Fig. 1. XRD pattern of CuO-αFe_2O_3 nanoparticles.

RESULTS AND DISCUSSION

X-ray Diffraction and SEM Analysis

Fig. 1 illustrates the X-ray diffraction (XRD) pattern of the CuO-αFe_2O_3 binary metal oxide. The diffraction peaks observed at (2θ) values of 38.83˚, 52.10˚, 59.45˚, 69.81˚, and 72.83˚ correspond to Miller indices (111), (020), (202), (220), and (311), respectively. These results align with the established diffraction data for CuO (JCPDS NO.01-1117). Additionally, peaks at (2θ) = 33.28˚ and 63.13˚, corresponding to the Miller indices (104) and (214) of αFe_2O_3, are consistent with the standard diffraction data (JCPDS NO.33-0664).

The incorporation of Fe_2O_3 into CuO induces discernible alterations in the XRD mixed pattern, suggesting a modification in the structural arrangement of CuO. The average crystallite size (D) was determined to be 13.96 nm using the standard Scherrer formula (Eq. 5) [20,22, 6].

$$D = \frac{k\lambda}{\beta \cos\theta} \quad (5)$$

Here, λ represents the XRD wavelength in nanometres, β is the mean width of the diffraction peak features at half maximum height due to small crystallite size in radians, and k is the crystallite form constant, typically set at 0.9.

In Fig. 2 FE-SEM images of synthesized CuO-αFe_2O_3 nanocomposite with surface morphology, shape and particle size. 30 The CuO-αFe_2O_3 at nanostructures form has a particle shape with diameter 13 to 23 nm. This size range correlates quite well with average crystal size (D), which had previously been obtained from XRD pattern data. The FE-SEM images provide important details on the microstructural properties of CuO-αFe_2O_3 nanocomposite and its dimensional characteristics.

Adsorption Experiments

Fig. 3 illustrates the impact of adsorbent concentration (ppm) on the removal efficiency of ALZ. The removal rate increases as the number of nanocomposites approaches the equilibrium limit, reflecting the increased availability of sorption sites until saturation occurs.

To optimize alizarin dye adsorption, the influence of contact duration on percent removal was investigated while keeping other parameters constant. As shown in Fig. 4, the adsorption of ALZ rises during the initial 90 minutes before reaching

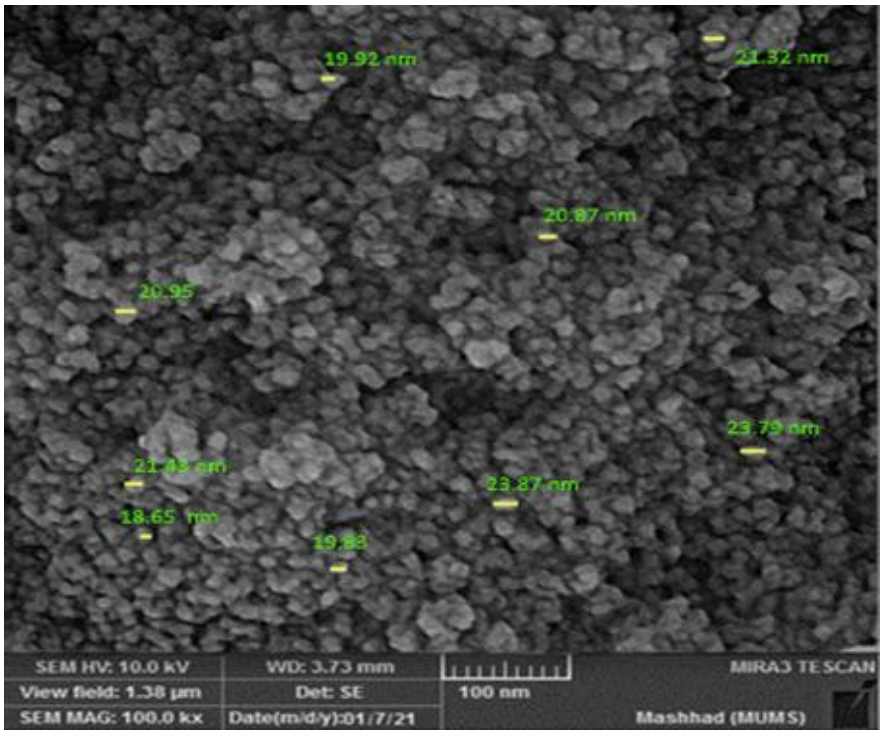

Fig. 2. FE-SEM image of CuO-αFe_2O_3 nanoparticles.

equilibrium. The rapid diffusion of ALZ to the external surface of CuO-αFe_2O_3 NPs within the first hour can be attributed to the nanoparticles' small size, facilitating efficient transfer of adsorbate species. As sorption sites become progressively filled, the adsorbed ALZ is transferred from the bulk solution to the occupied sorption sites. This delayed diffusion leads to a reduction in the rate of subsequent dye absorption.

When it comes to the adsorption isotherms, the

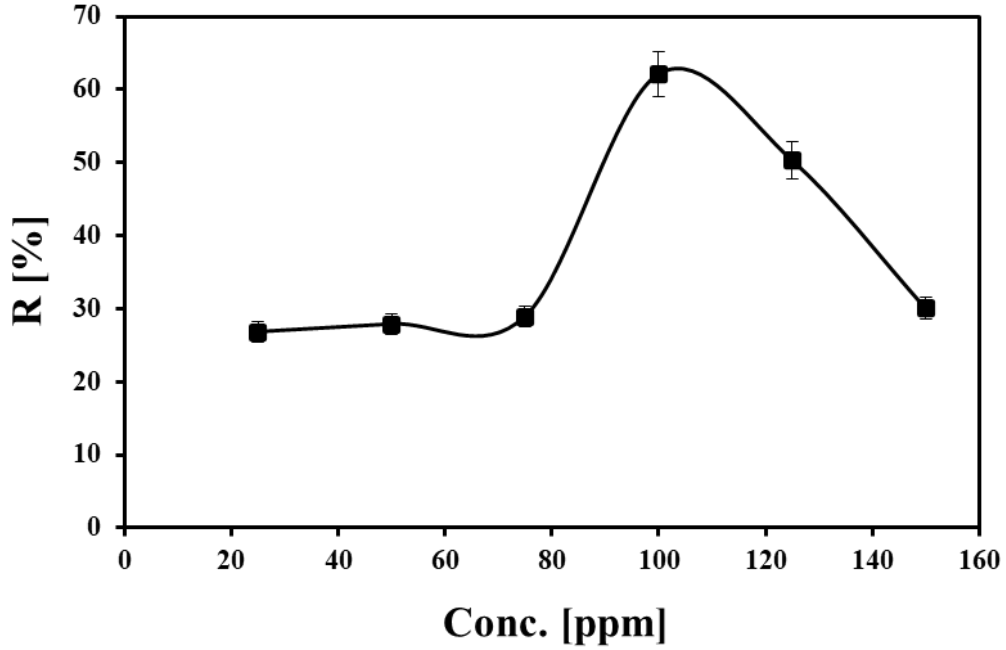

Fig. 3. Effect of adsorbent concentration (ppm) on the ALZ's removal efficiency.

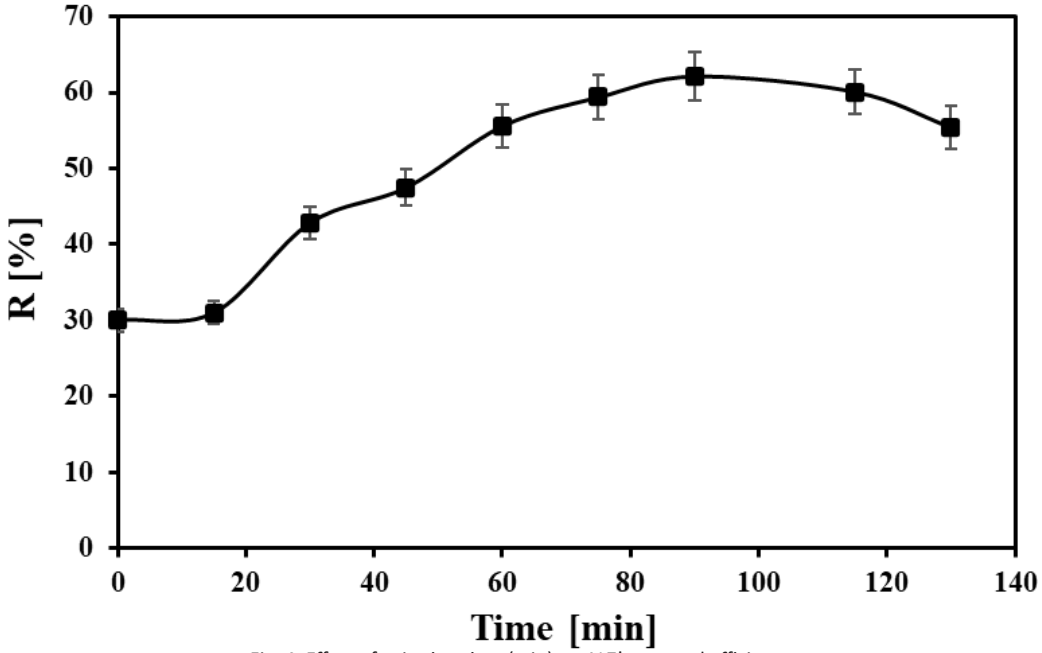

Fig. 4. Effect of agitation time (min) on ALZ's removal efficiency.

Langmuir equation did not fit the adsorption curve of alizarin red dye from its solution, as shown in Fig. 5a. The Freundlich equation, however, provided a suitable model for the desorption curve of alizarin red dye, as observed in the relationship between ln*Qe* and lnCe in Fig. 5b.

Thermodynamic Characteristics

The thermal influence on the adsorption process of alizarin red dye on the nanocomposite surface was investigated at various temperatures (20, 25, 30, 35, 40 °C). The results indicate an increase in the quantity of adsorbed alizarin red dye with rising temperatures, suggesting an endothermic process with a positive average value of enthalpy (ΔH). This supports the presence of an absorption system in relation to the adsorption process. The plot in Fig. 6, showing the relationship between logx_e and 1/T for ALZ adsorption, allowed for the calculation of entropy (ΔS) using the intercept method and maximum adsorbed species (x_m) using the slope of the van Hoff plot [34].

The calculated values for enthalpy (ΔH) and entropy (ΔS) were 20.7 kJ.mol^{-1} and -71.9 J.mol^{-1}K^{-1}, respectively. The adsorption isotherm at 313 K yielded a computed value of 21.1 kJ.mol^{-1}.K^{-1}, indicating that the adsorption occurs spontaneously without external force.

Theoretical Calculations

The equilibrium geometry of ALZ, as determined by the most efficient measurement (DFT), is presented in Fig. 7a. Table 1 presents the HOMO and LUMO energies along with the energy gaps for Alizarin, CuO-αFe_2O_3, and the Alizarin-CuO-αFe_2O_3 combination. The energy gap represents the difference between the energy values of the HOMO and LUMO orbitals, which

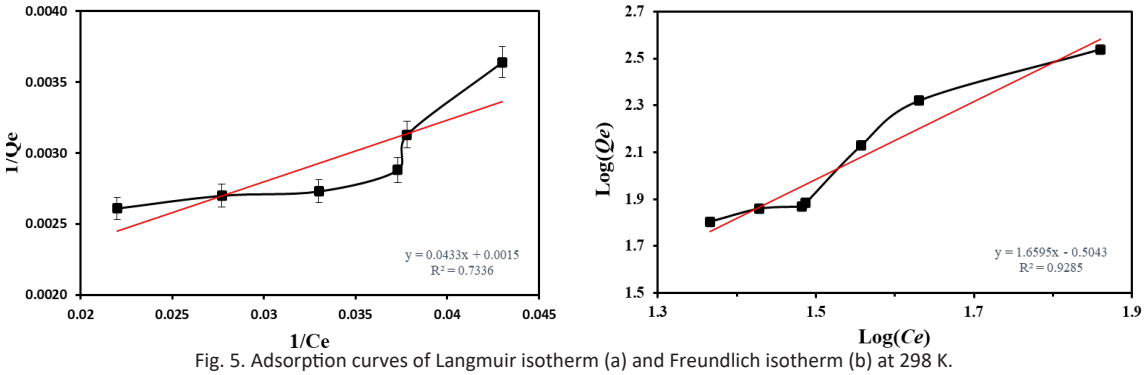

Fig. 5. Adsorption curves of Langmuir isotherm (a) and Freundlich isotherm (b) at 298 K.

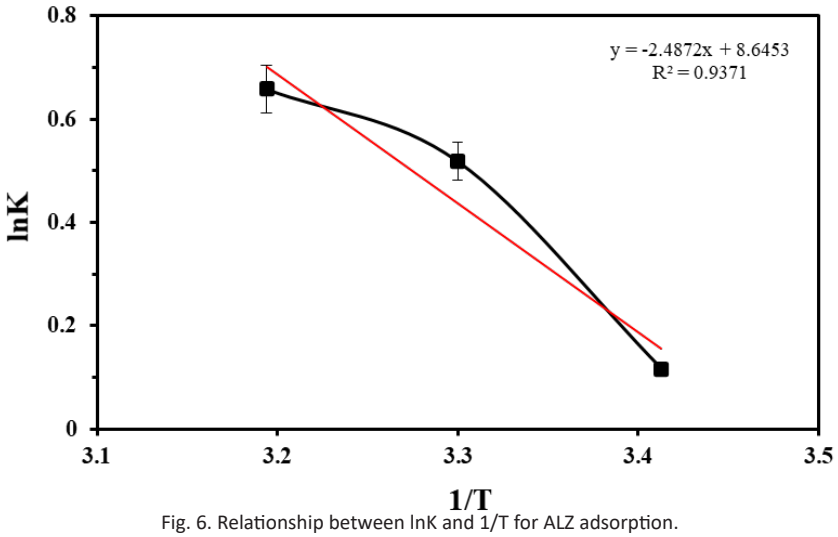

Fig. 6. Relationship between lnK and 1/T for ALZ adsorption.

serves as a valuable clue in determining the chemical reactivity and kinetic stability of the studied molecules.[31] An examination of the results reveals a significant alteration in the HOMO and LUMO energies attributed to the adsorption of the Alizarin molecule (Fig. 8). This impact suggests the involvement of chemisorption adsorption.[32] Furthermore, the energy gap expanded from 1.49

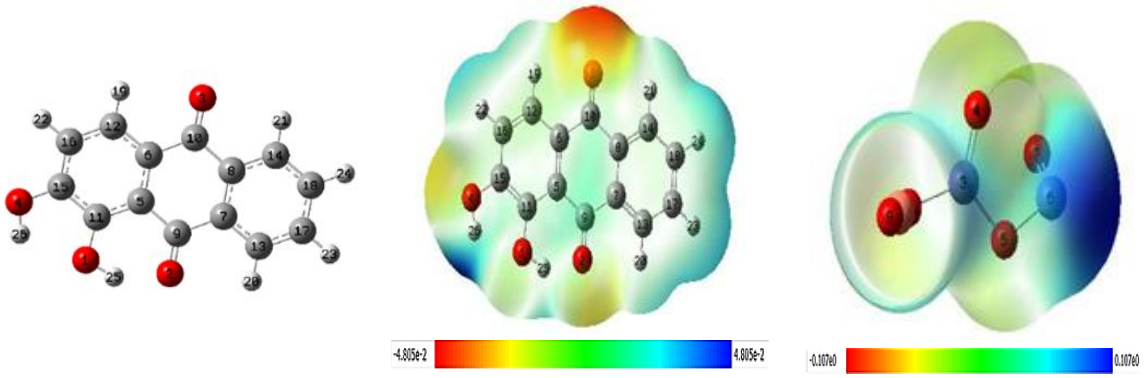

Fig. 7. The optimized structure of the ALZ molecule (a) as well as the electron density distribution of ALZ (b) and CuO-αFe$_2$O$_3$ nanocomposite (c).

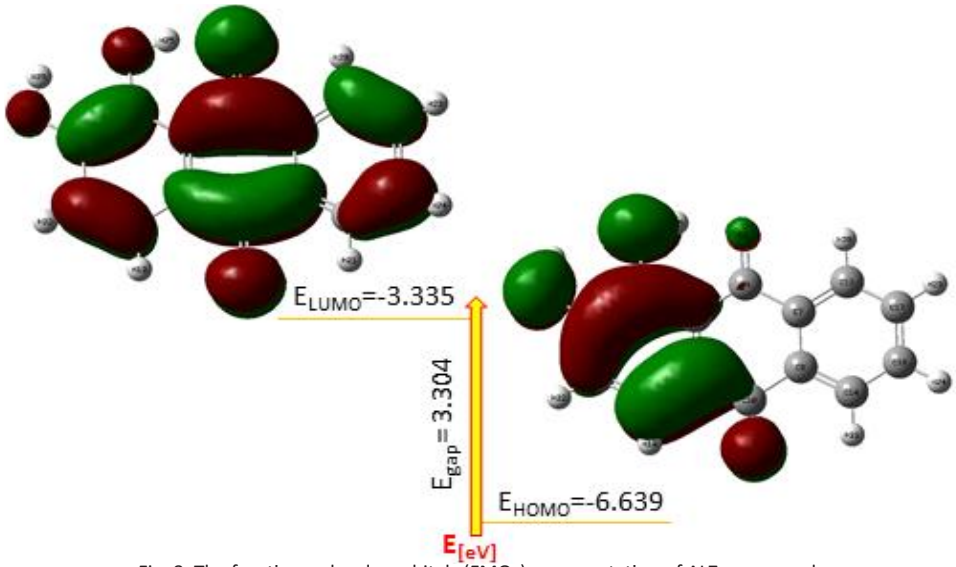

Fig. 8. The frontier molecular orbitals (FMOs) representation of ALZ compound.

Table 1. HOMO, LUMO, and Energy Gap Values (in eV) of Alizarin, CuO-αFe$_2$O$_3$, and their Resultant Complex Calculated at the B3LYP 6-311^{++}G(d,p).

System	E_{HOMO} [eV]	E_{LUMO} [eV]	ΔE [eV]
Alizarin	-6.64	-3.34	3.30
CuO-αFe$_2$O$_3$	-6.74	-5.26	1.49
Alizarin-CuO-αFe$_2$O$_3$	-5.99	-3.50	2.49

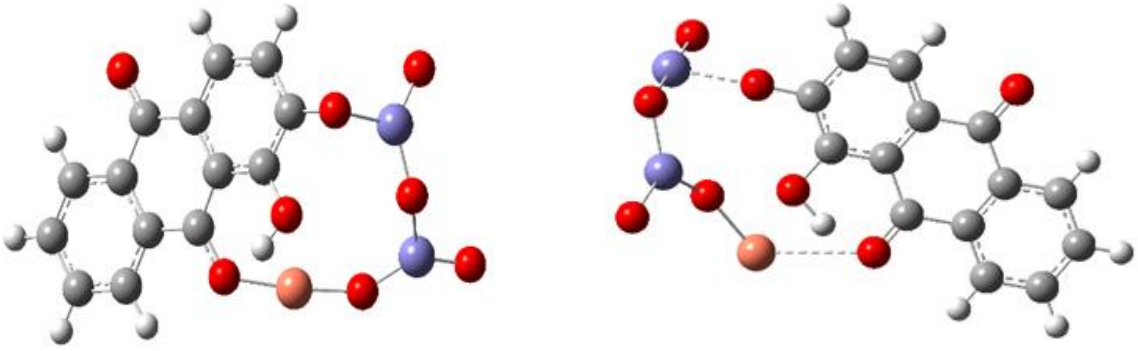

(a) (b)

Fig. 9. Optimized structures of ALZ–CuO-αFe2O3 after different types of adsorptions, as determined by DFT calculations: (a) chemisorption and (b) physisorption. Hydrogen, carbon, oxygen, iron, and copper atoms are depicted in white, grey, red, purple, and orange, respectively.

Table 2. Total energy (E) for CuO-αFe$_2$O$_3$, Alizarin-CuO-αFe$_2$O$_3$, and AlZ along the energy difference (ΔE) for both physisorption and chemisorption.

Adsorption type	ECuO-αFe$_2$O$_3$ [H]	EALZ-CuO-αFe$_2$O$_3$ [H]	EALZ [H]	ΔE [H]
physisorption	-4553.85	-5355.24	-839.47	38.08
chemisorption	-4553.85	-5307.32	-839.47	75.99

eV (CuO-αFe$_2$O$_3$) to 2.49 eV (Alizarin-CuO-αFe$_2$O$_3$ complex), indicating that the generated Alizarin-CuO-αFe$_2$O$_3$ complex is considerably more stable than isolated CuO-αFe$_2$O$_3$.

Moreover, to assess nucleophilic and electrophilic attack sites, electron density distribution on the optimal geometries of adsorbate and adsorbent molecules was computed. The molecular electrostatic potential (MEP) of Alizarin and CuO-αFe$_2$O$_3$, as depicted in Fig. 7b and Fig. 7c, revealed that oxygenated functional groups of Alizarin exhibited a large negative electron density (red colour), indicating nucleophilic attacking sites. In contrast, the metal atoms of CuO-αFe$_2$O$_3$ displayed a large positive electron density (blue colour), suggesting sites susceptible to electrophilic assault. The adsorption mechanism involves interactions between oxygen-containing nucleophilic groups and electrophilic atoms of the adsorbent [38, 39].

Comparing energies (E values) for a proposed linkage between the surface and the inhibitor facilitated the anticipation of adsorption types. Optimization operations using the DFT approach were performed for the surface (CuO-αFe$_2$O$_3$), Alizarin, and (Alizarin-CuO-αFe$_2$O$_3$). The covalent link in Alizarin-CuO-αFe$_2$O$_3$ was considered a chemical bond in the first state, while other states were assumed to be physical interactions as visualized in Fig. 9. Based on total electron density (TED) and electrostatic surface potential (ESP) calculations, the oxygen atom emerged as the active site in these interactions.

The adsorption type was deduced as physical, with ΔE values indicating physisorption and chemisorption. In chemisorption, ΔE equalled 75.99 H, while in physisorption, it was equal to 38.08 H (Table 2). The linkage between the dye and the surface, illustrated in Fig. 8, supported the theoretical understanding of the adsorption process.

CONCLUSION

The physical characterization of the synthesized CuO-αFe$_2$O$_3$ nanocomposite using XRD and SEM shows its nanoscale diameter. The adsorption of Alizarin red studies fitted the model by Freundlich's isotherm, and this research demonstrated that free-standing layer-thin nanocomposite has a great efficiency as an adsorbent. Thermodynamic

parameters support favourable adsorption and DFT calculations show a chemical state as well as physical interactions of the Alizarin–CuO-αFe$_2$O$_3$ link in two subsequent states. Importantly, in these interactions the oxygen achingly emerges as the active site. The high value of energy from the investigation indicates that physical adsorption is still the dominant type. The integration of experimentation and theory provides valuable insights into the adsorption of alizarin red over CuO-αFe$_2$O$_3$, thus advancing the knowledge on adsorption through a nanocomposite-powered approach.

ACKNOWLEDGEMENT

We would like to thank Mustansiriyah University, Baghdad, Iraq.

CONFLICT OF INTEREST

The authors declare that there is no conflict of interests regarding the publication of this manuscript.

REFERENCES

1. Lin X, Tang J, Zhu C, Wang L, Yang Y, Wu Ra, et al. Solvent-mediated precipitating synthesis and optical properties of polyhydrido Cu$_{13}$ nanoclusters with four vertex-sharing tetrahedrons. Chemical Science. 2023;14(4):994-1002.
2. Farhana NK, Omar FS, Mohamad Saidi N, Ling GZ, Bashir S, Subramaniam R, et al. Modification of DSSC Based on Polymer Composite Gel Electrolyte with Copper Oxide Nanochain by Shape Effect. Polymers. 2022;14(16):3426.
3. Jasim BE, Aboud NAA, Rheima AM. Nickel oxide nanofibers manufactured via sol-gel method: synthesis, characterization and use it as a photo-anode in the dye sensitized solar cell. Digest Journal of Nanomaterials and Biostructures. 2022;17(1):59-64.
4. Barhoumi A, Ourhriss N, Belghiti ME, Chafi M, Syed A, Eswaramoorthy R-m, et al. 3-Difluormethyl-5-carbomethoxy-2,4-pyrazole: Molecular mechanism of the formation and molecular docking study. Current Chemistry Letters. 2023;12(3):477-488.
5. Łapczuk-Krygier A, Kącka-Zych A, Kula K. Recent progress in the field of cycloaddition reactions involving conjugated nitroalkenes. Current Chemistry Letters. 2019:13-38.
6. Zhang H, He C, Han S, Du Z, Wang L, Yun Q, et al. Crystal facet-dependent electrocatalytic performance of metallic Cu in CO2 reduction reactions. Chin Chem Lett. 2022;33(8):3641-3649.
7. Rehman Ku, Zaman U, Khan D, Khan WU. Surfactant assisted CuO/MCM-41 nanocomposite: Ultra efficient photocatalyst for degradation of methylene blue dye and inactivation of highly drug resistant bacteria. Materials Chemistry and Physics. 2022;277:125454.
8. Dong Y, Yuan X, Zhou S, Tan H, Ma Z, Wang X, et al. Electrochemically incorporated Cu nanoparticles in NaVO3 with enhanced sodium-ion battery performance. J Power Sources. 2021;513:230535.
9. Abu-Zaid A, Abu-Zaid S, Barakat M, Al-Huniti R, Khair H. Figure 2 from: Abu-Zaid A, Abu-Zaid S, Barakat M, Al-Huniti R, Khair H (2024) Effectiveness of combination therapy of magnesium, vitamin B2 and Co-enzyme 10 supplementation on vestibular migraine: a retrospective cohort study. Pharmacia 71: 1-7. https://doi.org/10.3897/pharmacia.71.e112909. Pensoft Publishers; 2024. http://dx.doi.org/10.3897/pharmacia.71.e112909.figure2
10. Hamud WM, Al-Karawi AJM, Al-Kinani EM, Al-Sarray AJA. Removal of proflavine sulphate dye from wastewater using tea-bag tissue as an adsorbent. Desalination and Water Treatment. 2024;320:100613.
11. Kozlovskiy AL, Egizbek K, Zdorovets MV, Abdinov RS, Kadyrzhanov KK. Study of structural features and phase transformations in nanocomposites of Fe$_2$O$_3$@NdFeO$_3$ type. Journal of Materials Science: Materials in Electronics. 2021;32(16):21237-21247.
12. Popov N, Bošković M, Perović M, Németh Z, Wang J, Kuang Z, et al. Influence of low-spin Co^{3+} for high-spin Fe^{3+} substitution on the structural, magnetic, optical and catalytic properties of hematite (α-Fe$_2$O$_3$) nanorods. Journal of Physics and Chemistry of Solids. 2021;152:109929.
13. Tanuja G, Ganiger SK, Shashidhar S, Preeti RK, Patil SR, Lagashetty A. Solid state synthesis, characterization and biological evaluation of silver doped nanosized metal oxides. Current Chemistry Letters. 2023;12(4):821-830.
14. Al-Sarray AJA, Jasim BE, Aboud NA-A, Moaen FJ. Enhancing the Photostability of Poly(Vinyl Chloride) (PVC) Through the Incorporation of Cerium and Samarium Oxide. Polymer Korea. 2024;48(2):188-194.
15. Sukul PK, Kar C. Green Conversion Methods to Prepare Nanoparticle. Bioinspired and Green Synthesis of Nanostructures: Wiley; 2023. p. 115-139.
16. Gupta D, Boora A, Thakur A, Gupta TK. Green and sustainable synthesis of nanomaterials: Recent advancements and limitations. Environ Res. 2023;231:116316.
17. Abu-Zaid A, Abu-Zaid S, Barakat M, Al-Huniti R, Khair H. Figure 1 from: Abu-Zaid A, Abu-Zaid S, Barakat M, Al-Huniti R, Khair H (2024) Effectiveness of combination therapy of magnesium, vitamin B2 and Co-enzyme 10 supplementation on vestibular migraine: a retrospective cohort study. Pharmacia 71: 1-7. https://doi.org/10.3897/pharmacia.71.e112909. Pensoft Publishers; 2024.
18. Badran I, Khalaf R. Adsorptive removal of alizarin dye from wastewater using maghemite nanoadsorbents. Sep Sci Technol. 2019;55(14):2433-2448.
19. Al-Kadhi NS, Al-Senani GM, Algethami FK, Shah RK, Saad FA, ur Rehman K, et al. Facile synthesis of MgO/ZnO nanocomposite for efficient removal of alizarin red S dye from aqueous media. Inorg Chem Commun. 2024;162:112233.
20. Liu Y, Liu Y, Ji C, Zhang Y, Wang Y, Qu R, et al. Fabrication of attapulgite/C$_3$N$_4$ hybridized metal organic framework nanocomposites by different strategies and study on adsorption properties for alizarin yellow GG. Powder Technol. 2022;397:117113.
21. Burakov A, Neskoromnaya E, Babkin A. Removal of the Alizarin Red S Anionic Dye Using Graphene Nanocomposites: A study on Kinetics under Dynamic Conditions. Materials Today: Proceedings. 2019;11:392-397.
22. Makkar P, Ghosh NN. A review on the use of DFT for the prediction of the properties of nanomaterials. RSC Advances. 2021;11(45):27897-27924.
23. Eurasian Chemical Communications.

24. Kaya S, Ikot AN, Kumar A, Şimşek S, Zhu M, Guo L. Computational methods used in corrosion inhibition research. Eco-Friendly Corrosion Inhibitors: Elsevier; 2022. p. 527-538.
25. Kang J, Zhang X, Wei S-H. Advances and challenges in DFT-based energy materials design. Chinese Physics B. 2022;31(10):107105.
26. Al-Gharbawi HSA, Mahdi MS, Al-sarray MNN, Al-sarray SJK. Antibacterial activity and wound healing properties of chitosan ana nanoparticle chitosan in rat. Experimental and Theoretical NANOTECHNOLOGY. 2025;9(S):27-38.
27. Alaa Abd ALZ, Fadel ZH, Al-Sarray AJA, Hussein IA, Al-Noor TH. Corrosion Inhibition of Carbon Steel C45 Using New Azo Derivative in HCl Solution: Synthesis, Potentiostatic Measurement, and DFT Studies. Russian Journal of Physical Chemistry A. 2024;98(13):3202-3211.
28. Mongkolsuttirat K, Buajarern J. Uncertainty evaluation of crystallite size measurements of nanoparticle using X-Ray Diffraction analysis (XRD). Journal of Physics: Conference Series. 2021;1719(1):012054.
29. Sumadiyasa M, Manuaba IBS. Determining Crystallite Size Using Scherrer Formula, Williamson-Hull Plot, and Particle Size with SEM. BULETIN FISIKA. 2018;19(1):28.
30. Li YY, Jiang ZN, Wang X, Zeng XQ, Dong CF, Liu HF, et al. Developing a robust thiadiazole derivative corrosion inhibitor for dynamic supercritical CO2 aqueous environment: Electrochemical tests and DFT calculations. Corros Sci. 2022;209:110695.
31. Shokuhi Rad A, Sani E, Binaeian E, Peyravi M, Jahanshahi M. DFT study on the adsorption of diethyl, ethyl methyl, and dimethyl ethers on the surface of gallium doped graphene. Appl Surf Sci. 2017;401:156-161.
32. Nagy B, Jensen F. Basis Sets in Quantum Chemistry. Reviews in Computational Chemistry: Wiley; 2017. p. 93-149.
33. Goerigk L, Grimme S. Double-hybrid density functionals. WIREs Computational Molecular Science. 2014;4(6):576-600.
34. Kooh MRR, Dahri MK, Lim LBL. The removal of rhodamine B dye from aqueous solution using Casuarina equisetifolia needles as adsorbent. Cogent Environmental Science. 2016;2(1):1140553.
35. jasim b, husain a, aboud n, rheima A. Aqueous solution decolorization utilizing low-cost activated carbon produced from agricultural waste. Egyptian Journal of Chemistry. 2023;0(0):0-0.
36. Tawfiq KM, Al Naymi HAS, Obaid SMH, Jarad AJ, Al-Noor TH, Al-Sarray AJ. Synthesis, Characterization, Molecular Docking, Cytotoxicity, and Antimicrobial Activity of Schiff Base Ligand and Its Metal Complexes. Appl Organomet Chem. 2024;39(1).
37. Lassoued K, Seydou M, Raouafi F, Larbi F, Lang P, Diawara B. DFT study of the adsorption and dissociation of 5-hydroxy-3-butanedithiol-1,4-naphthaquinone (Jug-C4-thiol) on Au(111) surface. Adsorption. 2018;24(2):191-201.
38. Abou NA-A, Kareem K, Al-Sarray AJ, Jasim BE, Al-baghdadi SB, Ahmed AA. Synergistic Effect of ZnO/Chitosan Nanocomposite on the Photostability Enhancement of Polyvinyl Chloride. Polymer Korea. 2025;49(2):246-252.